International Journal of Mass Spectrometry and Ion Processes, 103 (1991) 117–128
Elsevier Science Publishers B.V., Amsterdam

A TRANSVERSALLY AND LONGITUDINALLY FOCUSING TIME-OF-FLIGHT MASS SPECTROMETER

R. KUTSCHER, R. GRIX, G. LI and H. WOLLNIK
II. Physikalisches Institut, Universität Giessen, 6300 Giessen (F.R.G.)
(First received 19 February 1990; in final form 28 May 1990)

ABSTRACT

The time-of-flight mass spectrometer described here has been designed for ions with angle and energy spreads as produced in a real ion source. It performs both transverse and longitudinal focusing. These focusing properties are achieved simultaneously by the inhomogeneous electrostatic field of a rotationally symmetric grid-free ion reflector with conically shaped entrance electrodes. When used in combination with a newly developed longitudinally focusing electron impact ion source, high sensitivity and high mass resolving power are obtained.

INTRODUCTION

Time-of-flight mass spectrometers (TOF-MSs) are of simple design. Linear TOF systems consist of an ion source, a drift path and an ion detector. The additional use of an ion reflector enables energy focusing. Many such systems have been developed and described (see for example refs. 1–15).

CONCEPTION

Principally, TOF-MSs require the formation of ion packets. These ion packets expand three-dimensionally in a field-free region owing to the angle and energy spreads of the ions and thereby usually limit the mass resolving power and the ion transmission of the mass spectrometer.

A new electron impact (EI) ion source [15] compresses the initial ion packets longitudinally to their shortest length at a certain distance from the ion source (see Fig. 1). This compression point can be viewed as the start point of the ion packets. The expansion of the ion packets after this compression point can be reversed by the inhomogeneous electrostatic field of a grid-free ion reflector. Optimally, the inhomogeneous field compresses the ion packets three-dimensionally, i.e. the ion reflector focuses the ions both longitudinally and transversally (see Fig. 1). Therefore the ion packets arriving at the detector are very similar to the ion packets at the compression point.

0168-1176/91/$03.50 © 1991 Elsevier Science Publishers B.V.

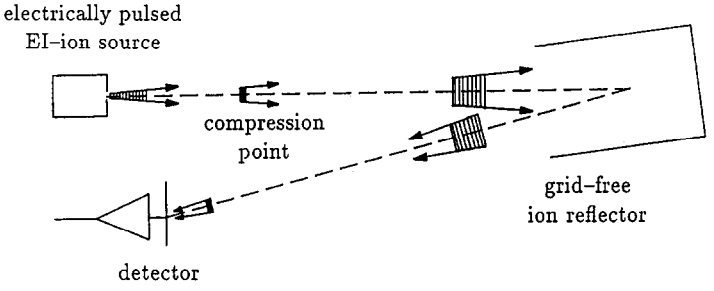

Fig. 1. Illustration of the three-dimensional expansion and compression of an ion packet at different positions during its flight in our TOF-MS. Leaving the ion source, the ion packet is first longitudinally compressed at the compression point. This ion packet then expands longitudinally and transversally until the grid-free ion reflector compresses the ion packet onto the detector in both the longitudinal and the tranverse directions.

THEORY

Ion source focusing

In order to bunch ion packets longitudinally the ions must be extracted from the ion source such that those of higher energy leave the ion source later than those of lower energy. At the beginning of the field-free region, therefore, ions of the lowest kinetic energy K_{min} are at the front and ions of the highest kinetic energy K_{max} are at the rear of an ion packet (see Fig. 2). Consequently all ions catch up with each other after a certain distance z_c, i.e. at the compression point. The spatial distribution of the kinetic ion energies between K_{min} and K_{max} determines the length of the ion packet at this compression point.

Ideally the ion packet length is zero at z_c, i.e. all ions have the same flight time to the compresson point z_c. Thus at the exit of the ion source the ideal

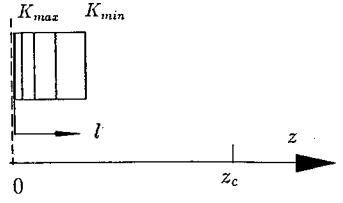

Fig. 2. Ideal spatial kinetic energy distribution of ions within an ion packet at the beginning of the field-free drift region. The vertical lines indicate ions of fixed energy with equal energy differences between ions of adjoining lines. This ideal spatial distribution $K(l)$ of eqn. (1) leads to an ion pulse length of exactly zero at the compression point.

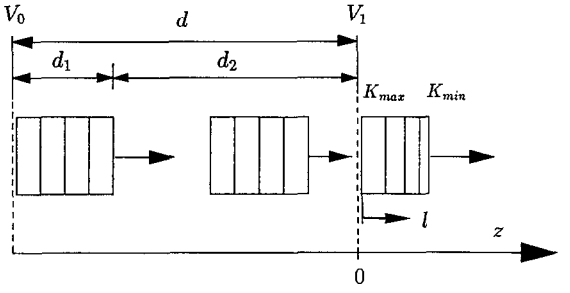

Fig. 3. Ions which are assumed to have started at different electrostatic potentials were accelerated constantly in the homogeneous electrostatic field $E = (V_1 - V_0)/d$. Therefore, in the field-free region they have different kinetic energies and also different distances between each other, which can be described by the function $K(l)$ of eqn. (2).

spatial distribution of the kinetic ion energy $K(l)$ is calculated as

$$\frac{K(l)}{K_{\max}} = \left(1 - \frac{l}{z_c}\right)^2 \tag{1}$$

where l is the distance to an arbitrary point downstream from the ion source (see Fig. 2). Consequently ions of higher energies are closer together than ions of lower energies (see Fig. 2).

Assume now that ions start at different electric potentials in a homogeneous electrostatic accelerating field $E = (V_1 - V_0)/d$ (see Fig. 3). On leaving this field the ions have different kinetic energies depending on their start potentials and the spatial distribution of the kinetic energies of the ions is calculated as

$$\frac{K(l)}{K_{\max}} = \frac{1}{2}\left[1 - \frac{l}{d} + \left(1 - \frac{2l}{d}\right)^{1/2}\right] \tag{2}$$

In this case the ions of lower energy are closer together than the ions of higher energy (see Fig. 3), contrary to the postulate of the ideal distribution of eqn. (1).

From the $K(l)$ of eqns. (1) and (2), one can obtain the inverse functions $l(K)$ and expand them in a power series in $\Delta K = K_{\max} - K$ as

$$l(K) = z_c\left[\frac{1}{2}\frac{\Delta K}{K_{\max}} + \frac{1}{8}\left(\frac{\Delta K}{K}\right)^2 + \cdots\right] \tag{3}$$

$$l(K) = d\left[\frac{\Delta K}{K_{\max}} - \frac{1}{4}\left(\frac{\Delta K}{K}\right)^2 - \cdots\right] \tag{4}$$

where $|\Delta K| \leqslant K_{\max} - K_{\min}$. Comparing eqns. (3) and (4), one finds that they

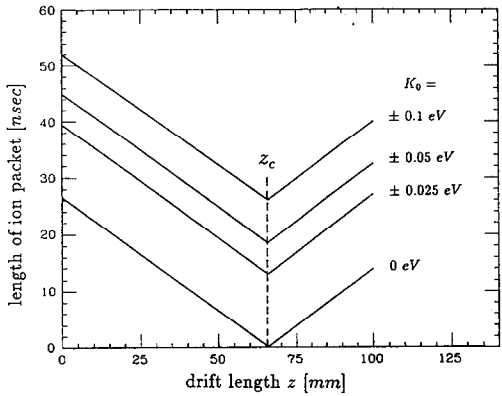

Fig. 4. The total ion pulse width is shown as function of the z coordinate in the field-free region for ions of mass $m = 28$ u and different thermal energies K_0. The ions start at different positions within a region $d_1 = 2$ mm and are accelerated over $d_2 = 30$ mm. The fields over the regions d_1 and d_2 are approximately identical. The ion pulse length for $K_0 = 0$ eV is only a few picoseconds.

are equal to first order if

$$z_c = 2d \tag{5}$$

Thus the distance between the electric field and the compression point z_c must be twice as long as the length d of the accelerating field.

To reduce the higher order contributions to eqns. (3) and (4), ΔK should be small as compared with K_{max} and the lengths of the ions packets in the electrostatic field be short as compared with the extension of this field. Therefore it is advantageous to divide the extension d of the electrostatic field into two parts with lengths d_1 and d_2 with $d_1 \ll d_2$ where d_1 is the region in which the ions are formed (see Fig. 3).

As eqns. (3) and (4) are not equal in higher order terms, the lengths of the ion packets at the compression point are not zero. From the numerical calculations one finds that the smallest length of the ion packet at the compression point z_c is achieved if the electrostatic field E_1 is only slightly less than E_2, where E_1 and E_2 are the field strengths over the distances d_1 and d_2 respectively.

Assuming that the ions formed at a certain position in the ion source all have the same initial thermal energies, the ion pulse length at z_c is only some picoseconds. However, if the initial thermal energies of the ions increase, the lengths of the ion packets at z_c increase considerably (see Fig. 4). In this case the lengths of the ion packets at the compression point are mainly determined by the time it takes for the ions, whose initial thermal velocities are opposite to the direction of the accelerating field, to reverse direction. This time is $2s/v$

where s is the distance the ion can move against the field E and v is the initial ion velocity. Numerically, one thus finds the time t (in nanoseconds) is given by

$$t \approx (Km)^{1/2}(70/E) \tag{6}$$

if K is in electronvolts, m in atomic mass units and E in volts per millimetre.

Grid-free ion reflectors

One-dimensional ideal ion reflector

The flight time in a TOF-MS is measured between the compression point and the final ion collector. Looking at single-mass ions only, the more energetic ones will require a shorter flight time than the less energetic ones. This effect can be compensated for by sending ions on a detour the length of which is designed such that the ion flight time becomes energy independent. Such detours can be achieved by using properly designed ion reflectors.

Most ion reflectors use homogeneous electrostatic fields formed between parallel grids [4,9,18]. We use grid-free reflectors which have the advantage that no wires exist in the beam. Thus there can be no charged surfaces close to ion trajectories and the field distributions are all smooth and show no ripple due to the wires in the grid. Unfortunately the optimization of grid-free ion reflectors requires more involved numerical calculations.

For such calculations, a field-free region is assumed to be followed by an arbitrary electrostatic field distribution in the ion reflector reaching up to a point $z_{\min}$, where the ions of lowest kinetic energy $K_{\min}$ reverse direction. The overall flight time t_{fixed} of these ions can then be calculated. In order to construct the ideal reflector field beyond $z_{\min}$, ions with a kinetic energy $K_{\min} + \mathrm{d}K$ with $\mathrm{d}K \ll K_{\min}$ are considered. The flight times of these ions to $z_{\min}$ are smaller than t_{fixed}. This time difference and the remaining energy $\mathrm{d}K$ determine the distances $\mathrm{d}z$ and a constant electrostatic field over a region $\mathrm{d}z$ that causes these ions to reverse direction. Increasing this ion energy by successive increments $\mathrm{d}K$ and repeating the calculation sequence, the field $E(z)$ can be calculated step by step up to any arbitrary kinetic ion energy. As the overall flight time is equal for all mono-mass ions, this one-dimensional ion reflector is ideal with respect to longitudinal focusing.

The potential distributions along the axis of rotation in two such one-dimensional ideal ion reflectors are shown in Fig. 5. Here the potential distribution beyond $z_{\min}$ depends on the arbitrary potential distribution up to $z_{\min}$. Consequently there are many possible field distributions for an ideal ion reflector.

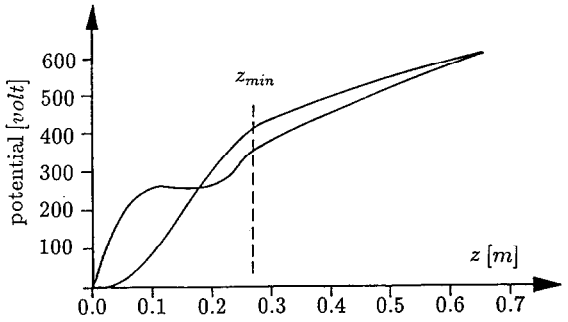

Fig. 5. Potential distributions along the axis of ideal ion reflectors. The potential distributions up to z_{min} (for the lowest ion energy) can be chosen arbitrarily. The potential distribution for larger z values are then calculated iteratively under the condition that the overall flight times of all ions of higher energy remain the same.

Three-dimensional grid-free ion reflectors

Once the potential distribution $V_0(z)$ along the axis of rotation of a grid-free ion reflector is known, the three-dimensional potential distribution can be determined using Laplace's equation:

$$V(r, z) = \sum_{k=0}^{\infty} \frac{(-1)^k \partial^{2k} V_0(z)}{(k!)^2 \partial z^{2k}} \left(\frac{r}{2}\right)^{2k}$$

$$= V_0 - \frac{1}{4} \frac{\partial^2 V_0(z)}{\partial z^2} r^2 + \frac{1}{64} \frac{\partial^4 V_0(z)}{\partial z^4} r^4 - \cdots \tag{7}$$

The potential $V_0(z)$ on this axis can be taken from a once-calculated one-dimensional ideal ion reflector. All ions moving along the axis of rotation are therefore energy focused longitudinally. However, this is not true for ions with different angles of inclination and different radial coordinates; nevertheless, this potential is a good approach to an optimal energy focusing for most incident ions and it can be improved iteratively to give good results for all ions of a beam.

In general, the three-dimensional inhomogeneous field distributions of grid-free ion reflectors have a second important property: the radial component of the electrostatic field strength can push the ions towards or away from the optical axis such that overall lateral focusing is achieved (see Fig. 6). It should be noted here that the focal length of such an ion reflector is shorter for higher ion energies, which is contrary to the case of transmitting electrostatic lenses. Consequently a combination of a transmitting electrostatic lens and an ion reflector can be used as an achromatic focusing device.

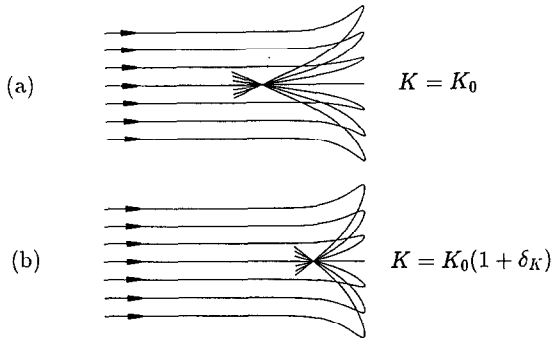

Fig. 6. Transverse focusing of the grid-free ion reflector for two different ion energies (a) and (b), where the ions for case (b) have higher energies than for case (a).

A transvere- and longitudinal-focusing ion reflector

We have developed a computer code [16] that iteratively optimizes the potential distribution in an ion reflector in order to achieve transverse and longitudinal focusing simultaneously. In Fig. 7 the calculated equipotential lines in such a reflector are shown, and ion trajectories are plotted for monoenergetic parallel incident ions. The diameter of the incident ion beam here is 60% of the aperture of the ion reflector. In the focal plane ($z = 0$ mm) the cross-sectional area of the reflected ion beam decreases to a small spot. The size of the spot in the focal plane represents the spherical geometric aberrations of the transverse focusing. If in addition different ion energies are considered, chromatic aberrations of the transverse focusing must also be considered.

In Fig. 8(a) the radial coordinates of the ions in the focal plane are plotted as a function of the relative ion energy deviations for ions originating from a

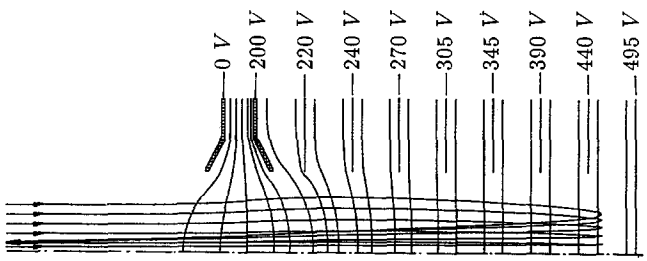

Fig. 7. Transverse focusing of the grid-free ion reflector used in the experiments. The ion reflector is rotationally symmetric with respect to the optical axis. The ion trajectories (450 eV ion energy) and the equipotential lines (40 V, 80 V, 120 V etc. up to 480 V) were calculated using a computer.

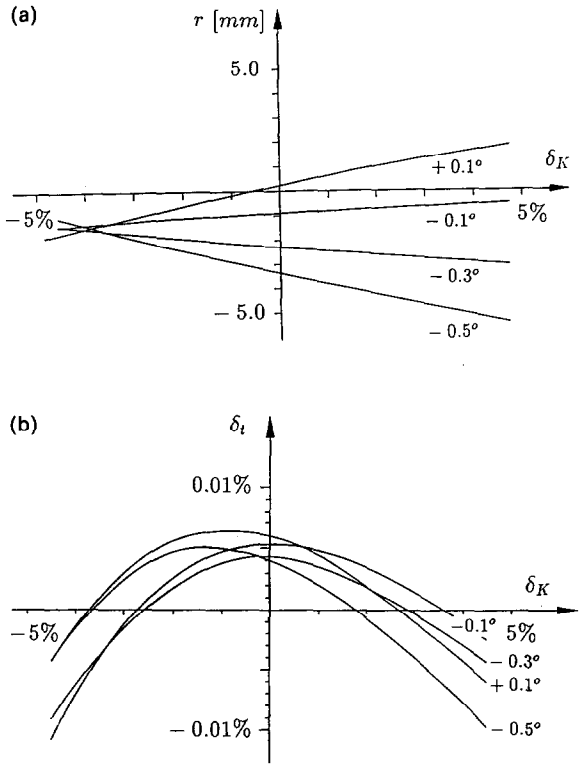

Fig. 8. (a) Calculated aberrations of the transversal focusing: the radial coordinate of the ion trajectories at the focal plane is plotted as a function of the relative ion energy deviation δ_K. The parameter is the angle of inclination of the incident ions. All ions were assumed to start 0.6 cm off the optical axis with a field-free region of 1.6 m before and behind the ion reflector. (b) Calculated aberrations of the longitudinal focusing: the relative aberration of the flight time is plotted as a function of the relative ion energy deviation δ_K. The parameter is the angle of inclination of the incident ions. T_0 is the flight time of a reference ion along the optical axis (inclination angle, 0°) with $\delta_K = 0$.

point-like ion source and passing through an ion reflector up to a final ion collector. For angles of inclination between $+0.1°$ and $-0.5°$ at the entrance to the ion reflector, the radial coordinate is widely independent of the ion energy deviation $\delta_K = \Delta K/K$, i.e. there is no substantial chromatic aberration for the transverse focusing. Varying the inclination angle for a certain ion energy ($0 \geqslant \delta_K \geqslant -4\%$), one finds that the spherical geometric aberrations of the transversal focusing are almost zero.

In a similar way the aberrations of the flight times of ions consist of chromatic and spherical aberrations because the overall flight time depends both on energy and angle (see Fig. 8(b)). Comparing Fig. 8(a) and Fig. 8(b)

one finds that in our case the optima of transverse and longitudinal focusing occur approximately simultaneously within the parameters. It should be noted here that we have chosen a conical shape of the entrance electrodes, as shown in Fig. 7, since we found better solutions in this case.

EXPERIMENTAL SET-UP

The ion source and the grid-free ion reflector described above were combined to form a TOF-MS, as indicated in Fig. 1. The vacuum manifold was evacuated with a $330\,l\,s^{-1}$ turbomolecular pump to a pressure of 10^{-7} mbar. The ions were generated by electron impact in the first stage of the ion source as described above (see Fig. 3).

The singly charged ions were accelerated to a kinetic energy of about 450 eV with an energy spread of about 10%. The ion packets with a minimum length at the compression point z_c were longitudinally and transversally focused onto the final ion detector by a grid-free ion reflector as shown in Fig. 7.

The ion detector consisted of two microchannel plates ($\phi = 25$ mm), the output of which was directly observed with a 350 MHz oscilloscope in order to see the mass spectra on-line. In addition, a transient recorder (Biomation 6500) was used to record single-shot spectra which were read to a PDP-11 computer.

EXPERIMENTAL RESULTS AND DISCUSSION

Transverse focusing

Firstly, a continuous ion beam was used to measure the transverse focusing of the grid-free ion reflector by using a Faraday cup 0.5 cm in diameter in a system in which the distance between ion reflector and final ion collector was about 1.5 m, and the beam in the ion reflector had a diameter of about 2 cm. The resulting ion current is shown in Fig. 9. To compare this beam cross-section with one formed by a two-stage ion reflector with homogeneous electrostatic fields (grid electrodes), we used such a reflector under identical conditions. In this case the ion intensity and thus the recorded ion intensity were considerably smaller (see Fig. 9).

The ion losses in the grid-free ion reflector are mainly caused by spherical aberrations, i.e. by ions entering the ion reflector close to the electrodes. Chromatic aberrations were very small so that ions of all energies were transmitted equally.

Longitudinal focusing

In all experiments the energy spread of the ions was larger than 10%. This large spread is deliberately produced by the ion source in order to achieve the

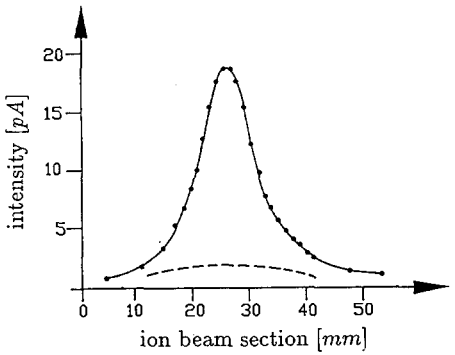

Fig. 9. Measurements of the beam cross-section of a continuous ion beam in the detector plane. The grid-free ion reflector curve (continuous line) is compard with the one (broken line) of a two-stage grid ion reflector with homogeneous electric fields recorded under otherwise identical conditions. It should be noted that the intensity distribution in the second case was wider than the range of the lateral coordinate shown here.

well-bunched ion packets. For this energy spread the longitudinal focusing of the grid-free ion reflector is so good that the ion pulse length at the detector is about the same as that measured at the compression point of the ion source [17]. The oscillogram in Fig. 10 shows the mass spectrum of the xenon isotopes recorded at a repetition rate of about 1 kHz. The peak widths (FWHM) are about 20 ns for total flight times of about 150 μs, yielding a mass resolving

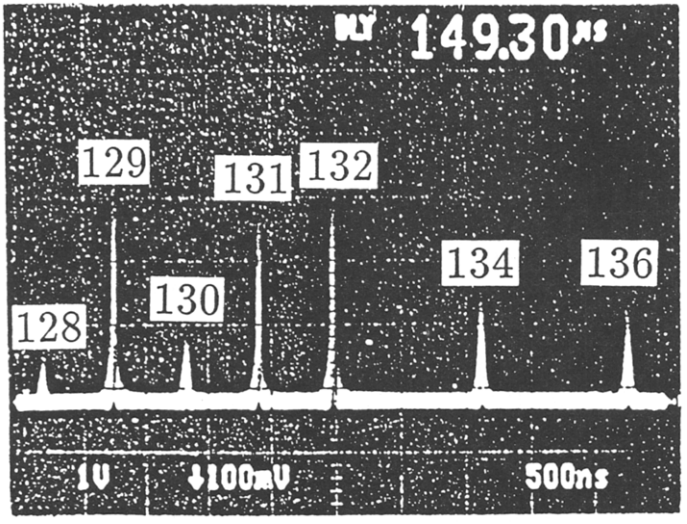

Fig. 10. A spectrum of Xe isotopes; in this oscillogram the mass resolving power is about 3500.

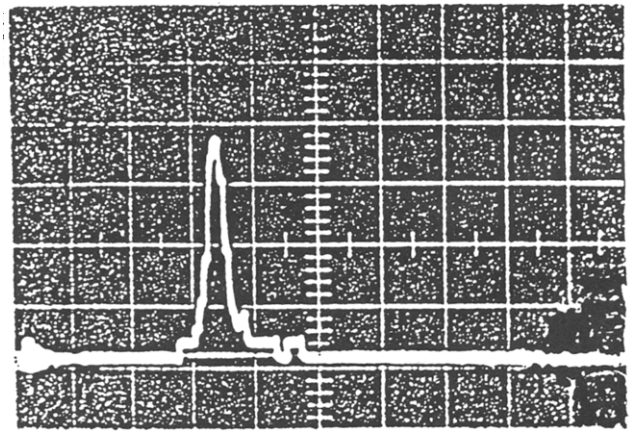

Fig. 11. An Xe mass line (m = 132) of a single-shot mass spectrum recorded by the transient record. The resolving power is about 10 000. The steps in the mass line correspond to the 2 ns channel width of the transient recorder.

power of about 3500. On closer examination the peaks of the on-line spectra are slightly blurred. A jitter of several nanoseconds (caused by instabilities of the electronic equipment) can be observed by lowering the repetition frequency. A single-shot mass spectrum recorded in a transient recorded yielded a mass resolving power of about 10 000 (see Fig. 11).

Reflector modes

An interesting property of the grid-free ion reflector is the fact that it can have two or even more modes, i.e. distinct electric field distributions, for which the ions are suitably reflected. In all these modes, longitudinal and transverse focusing can be observed. The intensities of the mass spectra differ only slightly and the mass resolving power remains about constant as long as not too high values are required. However, the mass spectra of different modes are shifted on the time scale, because the flight times within the ion reflector are varied by different field distributions.

For two modes, we measured the voltages of the electrodes of a grid-free ion reflector belonging to the same TOF-MS [15]. From these measurements we calculated the corresponding rotationally symmetric potential distributions in the reflector and obtained potential distributions along the reflector axis. These quite different distributions of the two reflector modes are shown in Fig. 12 and should be compared with those of an ideal ion reflector (see Fig. 5).

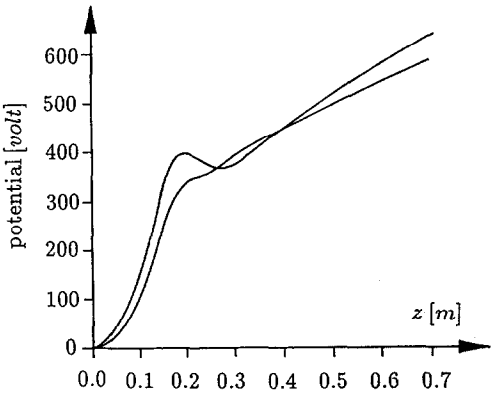

Fig. 12. Potential distributions along the optical axis for two reflector modes, calculated from measured potentials of the reflector electrodes.

ACKNOWLEDGEMENTS

Financial support of the Deutsche Forschungsgemeinschaft (DFG) is gratefully acknowledged.

REFERENCES

1 A.E. Cameron and D.F. Eggers, Rev. Sci. Instrum., 19 (1948) 605.
2 W.C. Wiley and I.H. McLaren, Rev. Sci. Instrum., 26 (1955) 1150.
3 R.S. Gohlke, Anal. Chem., 31 (1959) 535.
4 V.I. Karataev, B.A. Mamyrin and D.V. Shmikk, Sov. Phys. Tech. Phys., 16 (1972) 1177. B.A. Mamyrin, V.I. Karataev, D.V. Shmikk and V.A. Zagulin, Sov. Phys. JETP, 37 (1973) 45.
5 F. Hillenkamp, E. Unsöld, R. Kaufmann and R. Nitsche, Appl. Phys., 8 (1975) 431.
6 R.D. Macfarlane and D.F. Torgerson, Int. J. Mass Spectrom. Ion Phys., 21 (1976) 81.
7 B.T. Chait and K.G. Standing, Int. J. Mass Spectrom. Ion Phys., 40 (1981) 185.
8 U. Boesl, H.J. Neusser, R. Weinkauf and E.W. Schlag, J. Phys. Chem., 86 (1982) 4875.
9 W. Gohl, R. Kutscher, H.J. Laue and H. Wollnik, Int. J. Mass Spectrom. Ion Phys., 48 (1983) 411.
10 H. Danigel, H. Jungclas and L. Schmidt, Int. J. Mass Spectrom. Ion Phys., 52 (1983) 223.
11 R. Frey, G. Weiss, H. Kaminski and E.W. Schlag, Z. Naturforsch., Teil A, 40 (1985) 1349.
12 E. Niehuis, T. Heller, H. Feld and A. Benninghoven, Springer Proc. Phys., 9 (1986) 189.
13 X. Tang, R. Beavis, W. Ens, B. Schueller and K.G. Standing, Am. Soc. Mass Spectrom. 34th Ann. Conf. Cincinnati, OH, 1986, p. 171.
14 S. Della-Negra and Y. LeBeyec, Rapid Commun. Mass Spectrom., 1 (1987) 10.
15 R. Grix, R. Kutscher, G. Li, U. Grüner and H. Wollnik, Rapid Commun. Mass Spectrom., 2 (1988) 83.
16 J. Brezina, University of Giessen, personal communication (1986).
17 R. Grix, U. Grüner, G. Li, H. Stroh and H. Wollnik, Int. J. Mass Spectrom. Ion Processes, 93 (1989) 323.
18 D. Ioanoviciu, G.E. Yefchak and Ch. G. Enke, Int. J. Mass Spectrom. Ion Processes, 94 (1989) 281.